GEOPHYSICS, VOL. 89, NO. 1 (JANUARY-FEBRUARY 2024); P. WB13–WB23, 15 FIGS.
10.1190/GEO2023-0224.1

Detecting and recovering critical mineral resource systems using broadband total-field airborne natural source audio frequency magnetotellurics measurements

Alexander Prikhodko[1], Andrei Bagrianski[1], Robert Wilson[1], Sergey Belyakov[2], and Nurganym Esimkhanova[2]

ABSTRACT

Airborne geophysical methods offer a substantial advantage compared to ground-based techniques in exploring territories of different sizes, ranging from entire metallogenic provinces to the deposit scale, including those hosting critical minerals. An airborne method with measurements of natural magnetic field variations, known as audio frequency magnetotellurics (a passive field method), significantly increases the depth of investigation and expands the resistivity detection range compared with some controlled-source primary-field methods. We describe the technical solutions used in an airborne electromagnetic passive system with a mobile sensor of the total magnetic field variations and the stationary sensor of electric field variations, and its applications to recovering the complex geology of hydrothermal-magmatic systems often associated with critical minerals. The system's ability to explore depths, typically beginning from the near-surface and down to 1–2 km, by recording responses in three orthogonal inductive coils over a broad bandwidth from 22 Hz to 21,000 Hz allows for mapping resistivities across a broad range. This capability is crucial for obtaining more comprehensive exploration models. Field case studies of the natural field system include application in exploring for unconformity uranium mineralization, along with other associated minerals, epithermal gold and polymetallic-bearing structures, and ferromanganese and polymetallic deposits formed in a continental rift valley. An extra case study involving kimberlites was incorporated as a proven example of the natural field system's capability in conducting near-surface and deep investigations. The case histories illustrate the airborne natural electromagnetic field technology capabilities in recovering geoelectric models and their specific patterns.

INTRODUCTION

Airborne electromagnetics (AEM) is commonly used in mineral exploration programs to map resistivity and detect geologic targets of interest. However, AEM systems' different measurement principles and technical designs have varying advantages and limitations in their exploration capabilities and practical usage under different geoelectrical conditions. The depth of investigation of AEM systems with controlled primary-field sources is limited, particularly in conductive environments or in the presence of conductive overburden, and is highly dependent on system orientation (Allard, 2007). Furthermore, the detectable range of resistivity for most common "off-time" time-domain systems only covers the range of resistivity variations, approximately, below 1000 Ωm, and is limited in the detection of highly conductive mineral assemblages (Annan et al., 1996; Smith, 2001), although the use of "on-time" data can potentially expand the time-domain detectability range by about a decade at the high- and low-conductivity extremes

Manuscript received by the Editor 14 April 2023; revised manuscript received 26 August 2023; published ahead of production 25 September 2023; published online 12 December 2023.
[1]Expert Geophysics Limited, Aurora, Ontario, Canada. E-mail: alexander@expertgeophysics.com (corresponding author); andrei@expertgeophysics.com; robert@expertgeophysics.com.
[2]Qazaq Geophysics, Zhezkazgan, Kazakhstan. E-mail: sergey.belyakov@kazakhmys.kz; nurganym.esimkhanova@kazakhmys.kz.

(Smith and Annan, 1998). Diagnostic limitations also exist in a "tipper" type of audio frequency magnetotellurics (AFMAG) system, which is only sensitive to conductivity contrasts, not absolute conductivities, limiting the ability to obtain a comprehensive geoelectrical characterization (Jansen and Cristall, 2017). In addition, some "tipper" type systems can lack a remote reference station (used for providing bias-free data) and have a limited frequency bandwidth with a comparatively small number of frequencies (Legault et.al., 2009; Lo et al., 2009). Furthermore, any required tilt corrections for the data of a single component can be imprecise (Kuzmin et al., 2010), especially over rugged terrain.

The MobileMT system is a recent advancement in passive airborne electromagnetic technology. This airborne electromagnetic system exploiting natural electromagnetic (EM) fields is an efficient tool for mineral exploration in various geologic and geoelectrical terrains, with anomalous features evident on our sections at depths between 1 km and 2 km, depending on the environment's overall conductance. The broad bandwidth for recording responses has allowed us to obtain inverted (with 2D models) resistivities from 1 Ωm, confirmed by direct comparison with ground MT (Prikhodko et al., 2022), to 20,000 Ωm, in a field example presented subsequently. The case studies from MobileMT surveys are presented over areas with known and possible mineral deposits, occurrences, and mineralization-controlling structures. The recovered resistivity-depth images are compared with conceptual geologic models of the mineralization systems, which illustrate the system's capabilities in imaging mineralization-controlling structures and their diverse geometries and wide resistivity range.

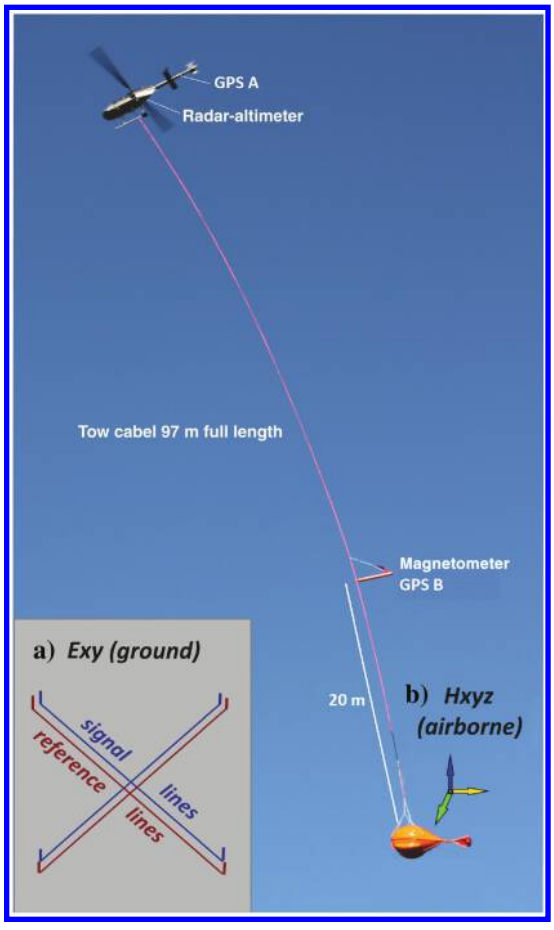

Figure 1. MobileMT system in survey configuration. (a) Schematic representation of a base station, which includes two pairs of independent grounded orthogonal electric lines in the same position, (b) shows a schematic representation of three orthogonal dB/dT inductive coils. These are in the tear-drop shaped housing (or bird) towed by a 97 m cable attached to a helicopter. The system also has a magnetometer to measure total magnetic intensity of the earth's field (not further discussed in this paper).

KEY TECHNICAL SOLUTIONS AND DATA PROCESSING

The operating principle of the airborne natural-field MobileMT EM technology is a combination of magnetotelluric (MT) and magnetovariational concepts (Prikhodko et al., 2022). The measuring system includes two main parts (Figure 1):

1) Three orthogonal dB/dT inductive coils fixed rigidly to each other (Figure 1b) in a drop-shaped shell towed 97 m below the helicopter. Variations of the magnetic field (H-field) measured by the inductive receiver are recorded digitally in an acquisition system placed inside a helicopter. It is unnecessary to monitor or control the tilt precisely because the measurement system provides total-field data.
2) Two pairs of independent grounded orthogonal electric lines positioned a few meters apart (Figure 1a) for measuring "main" and "reference" variations of the electric field (E-field). The electrodes separation is, typically, 100 m but depends on the natural signal level. The data from the stationary measurement system are recorded similarly to the mobile H-field acquisition system. One of the reasons for choosing electrical components for reference is the capacity to control the natural signal strength by changing the length of the dipoles.

The electrical base station consists of two orthogonal pairs of grounded lines with simultaneous but independent data acquisition channels. One is used as a reference for applying the cross-spectral technique, in a similar fashion to that described by Labson et al. (1985), to remove auto-power bias distortions. The denoised and corrected E-field data represent the primary natural EM field variations. They facilitate the separation of the time-variance from the space-variance of the measured fields (like in MV).

The preference for using electric field variations at the base station versus magnetic field is supported by field experiments in the Sierra Nevada of California, where the electric field reference was used "because the signal-to-noise ratio (S/N) for the electric field measurements was much higher than the S/N for the magnetic field" (Labson et al., 1985).

In addition, the combination of magnetic (**H**) and electric (**E**) fields variations allows the use of the concept of the admittance tensor introduced by Thomas Cantwell in 1960 as $\mathbf{Y} = \mathbf{H}/\mathbf{E}$ (Cantwell, 1960; Jones, 2017) and, ultimately, the calculation of apparent conductivities corresponding to different frequency bands:

$$\sigma(\omega) = \mu\omega|Y^2|, \tag{1}$$

where $\boldsymbol{\mu}$ is the magnetic permeability of free space and $\boldsymbol{\omega}$ is the angular frequency.

Having magnetic and electric field data variations measured in different relative orientations and in different relative directions, magnitudes of total **H** and **E** vectors independent of the sensors' spatial attitudes are calculated at the same frequency and time as

DOI:10.1190/geo2023-0224.1

$$|\mathbf{H}(f)| = \sqrt{(Hz(f)^2 + Hx(f)^2 + Hy(f)^2)}, \quad (2)$$

$$|\mathbf{E}(f)| = \sqrt{(Ex(f)^2 + Ey(f)^2)}, \quad (3)$$

where **f** is frequency, **H** and **E** are the total vectors of the magnetic and electric fields, $H(zxy)$ and $E(xy)$ are the magnetic and electric fields in orthogonal directions, respectively.

The calculations follow the methodology outlined by Kuzmin et al. (2010). However, in the MobileMT context, electric field components are used at the base station instead of using magnetic field components.

The vector components $\mathbf{H}(f)$ and $\mathbf{E}(f)$ are compared, and the attitude-invariant properties of the relating tensors are calculated. Like another AFMAG prototype, AirMT (Kuzmin et al., 2010, Prikhodko et al., 2022), the 3D vector of magnetic field variations can be correlated with changes in the vector derived from the horizontal components at a base station. However, in the case of MobileMT, the latter components are of the electric field. The relation between the two vectors $\mathbf{H}(f)$ and $\mathbf{E}(f)$ can be expressed through the 3×2 matrix tensor (**T**):

$$\begin{bmatrix} Hx \\ Hy \\ Hz \end{bmatrix} = \begin{bmatrix} TxxTxy \\ TyxTyy \\ TzxTzy \end{bmatrix} \begin{bmatrix} Ex \\ Ey \end{bmatrix}. \quad (4)$$

Given that the electromagnetic wave is treated as a plane wave, it is possible to establish a coordinate system for which the 3D magnetic complex vector can be represented as two 2D vectors, one real and one imaginary, with the third coordinate component set to zero. The resulting 2D vectors can be processed by known methods used in the ground MT method for processing 2D electric vectors (Vozoff, 1972) and incorporating of a reference signal (Anav et al., 1976). In the result of the processing, a determinant of the **T** matrix defining relation between the $\mathbf{H}(f)$ and $\mathbf{E}(f)$ vectors is calculated. This determinant is independent of the sensors (ground and in the air) orientation and reflects the relationship between signal energies at ground and airborne survey locations. It is one in homogeneous regions but changes in the presence of lateral conductivity variations (Kuzmin et al, 2010). Because the rotation invariant parameters do not require an attitude correction to remove the mixing effect of horizontal fields with vertical field components, the S/N is higher than in tipper measurements in the air (Legault and Fisk, 2012). During an aerial survey, the distance between the magnetic and electric field receivers varies between a few and 30–40 km. Measurements at longer distances have yet to be tested. However, a very long separation between the receivers will most strongly affect data corresponding to high frequencies, which may be critically important depending on the exploration task and geoelectrical conditions.

The EM field variations are measured in 22 Hz–21 kHz frequency range. The natural EM field in this frequency range is primarily a consequence of atmospheric electric discharges that accompany thunderstorms on a global scale (Labson et al., 1985). The time-series data (Figure 2) are digitized and recorded at a 73,728 Hz sampling rate, with data synchronized by the global positioning system (GPS) timing. One measurement "station" along a survey line results from time series data acquisition, conversions to the frequency domain and averaging of the resulting data for 1.5 s or 2 s (selectable). The averaging results in a 40–50 m station spacing at 90 km/hour the nominal aircraft speed. The distance between stations in the final databases is usually 12–15 m (depending on the flight speed), resulting from the continuously moving and overlapping time window (1.5 or 2 s) during the time series processing.

The signals of two denoised horizontal electric components, and three magnetic components, are processed with the MT response functions based on linear relations between components of the electric and magnetic fields. The fast Fourier transform technique is applied to the merged recordings with the calculation of six admittance matrices of the relations between the magnetic and electrical signals in a set of serial frequency windows. The total frequency range is typically divided into 30 windows, as shown in Figure 3. The frequency window widths correspond to the length of the vertical lines on the graph. The frequency windows and their centers are customizable depending on the frequency of anthropogenic sources and other external noise if it exists.

The actual set of frequencies accepted for the final databases depends on the natural signal strength during each survey and the characteristics of external electromagnetic noise if present. The typical number of accepted apparent conductivities for a survey is in the range of 12–20.

Station-to-station static correction of the airborne EM data is not required due to the constant position of the E-field measurement system and the absence of measurements of galvanically distorted electric fields between stations. However, the static shift between survey blocks with different positions of the E-field base station is essential (Sattel et al., 2019). Prior resistivity data from a survey

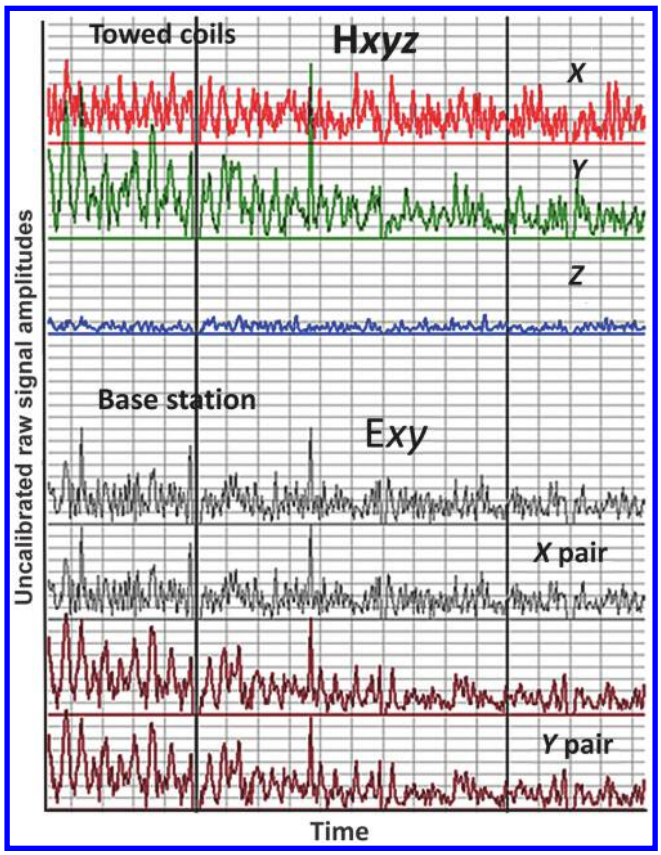

Figure 2. Time series data recorded simultaneously during approximately 30 ms by three orthogonal inductive coils in the air (H-field) and by two orthogonal pairs of grounded lines (E-field).

region can be used as a reference for overall data calibration. In practice, apparent conductivity data calibration, or correction, is not required when more-or-less uniform overburden covers an area. However, it is essential when comparatively significant changes in the near-surface geoelectrical conditions exist. Apparent conductivities acquired during MobileMT surveys, such as the field examples in the paper, are checked to see if their average resistivity is consistent with the known or estimated average in a region.

This airborne electromagnetic technology offers several advantages, such as: (1) its ability to investigate a wide depth range (from the near-surface to 1–2 km and deeper if a geologic environment is highly resistive); (2) sensitivity to geoelectrical boundaries in any direction (from horizontal to vertical); (3) sensitivity across a broad range of resistivities (confirmed by direct comparison with ground MT and recovered in 2D models) from 1 Ωm (Prikhodko et al., 2022) to approximately 20,000 Ωm, in the case study from the Athabasca Basin subsequently); and (4) high spatial and depth resolution. Furthermore, the MobileMT data output relies less on terrain clearance than systems with controlled-source transmitters. Figure 4a shows the variation of the receiver altitude over an area with very rugged relief (between 2700 m and 4000 m above sea level, ASL) and the calculated apparent conductivities corresponding to low (Figure 4b) and high frequencies (Figure 4c). There is negligible influence of the terrain clearance on the apparent conductivity data. In more typical surveys, the nominal receiver height above the surface is 60–70 m.

Data from MobileMT surveys have been compared directly with other airborne EM technologies, and MobileMT, with its broad range of frequencies, is capable of covering the depth range generally achieved by three other methods — tipper AFMAG, time-domain and very low frequency (VLF) (Moul and Witherly, 2020). A comparison of MobileMT and airborne time-domain controlled-source data (Figure 5) shows a strong correlation between geologic features evident on the color grid generated from 256 Hz MobileMT window and profiles from a roughly comparable time window measured with the VTEM ATDS system. In this case, the tops of conductive zones in the area are located between 70 m and 120 m, as interpreted from a

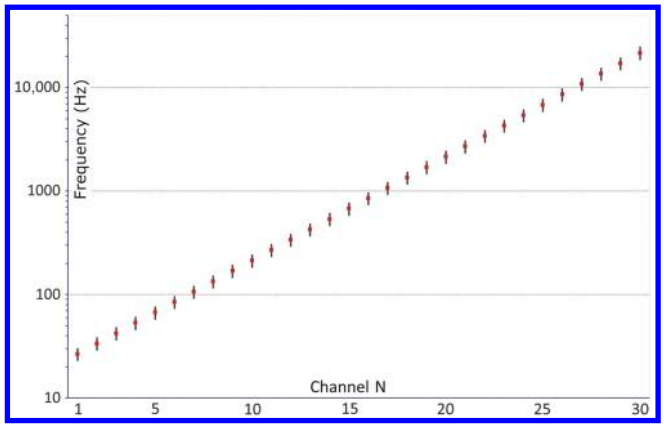

Figure 3. Typical MobileMT data frequency windows with centers from 26.3 at the channel 1 to 21,542.5 Hz at the channel 30.

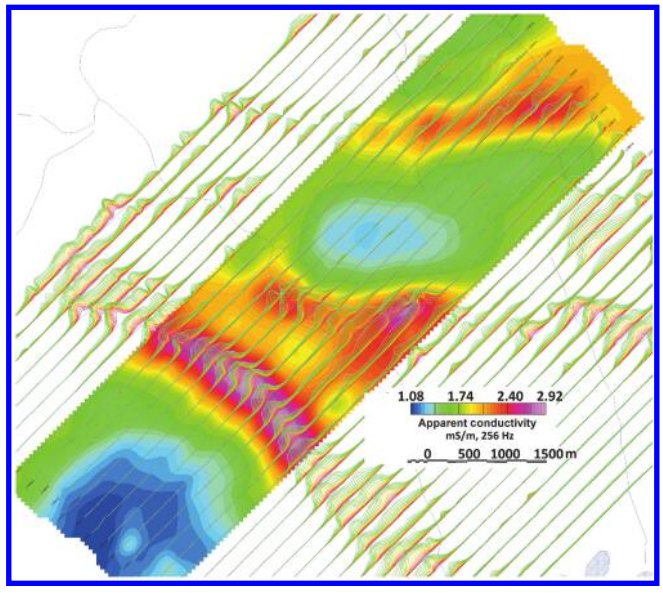

Figure 5. MobileMT apparent conductivity color grid (256 Hz) with overlapped VTEM dB/dt profiles in the 0.145–1.333 ms off-time range in the log-linear scale with the largest amplitude 17.5 pV/(A * m^4) (Porcupine mining district, Ontario, Canada).

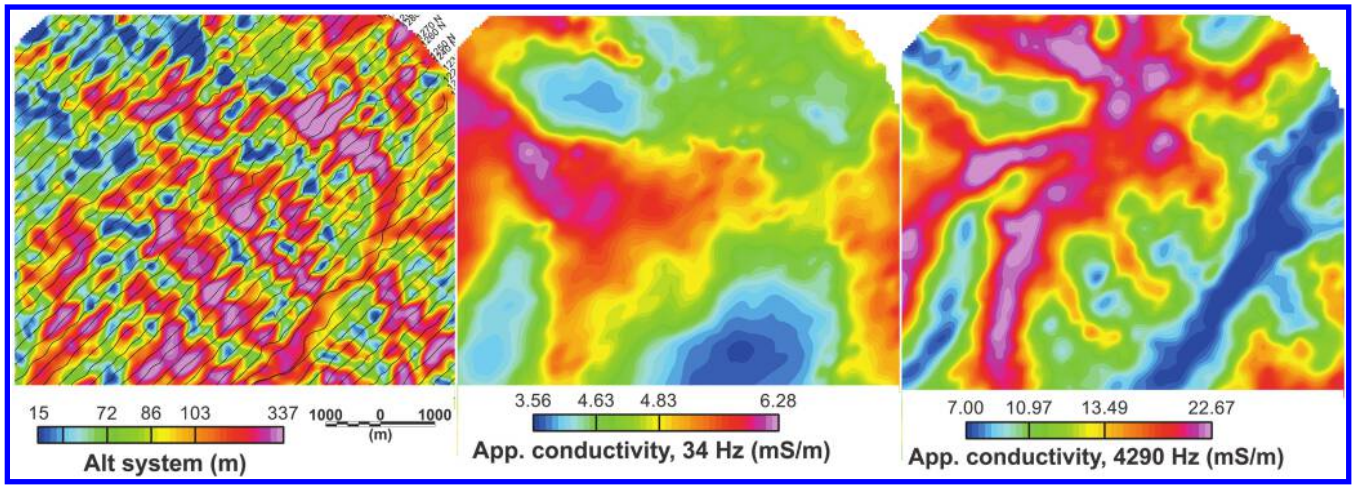

Figure 4. Illustration of the lack of artifacts associated with terrain clearance on the calculated apparent conductivity data: (a) distance between MobileMT H-field receiver and the surface over a survey area; (b) apparent conductivity color grid, from 34 Hz data; and (c) apparent conductivity color grid, 4290 Hz. These data are from a MobileMT survey in Colorado.

DOI:10.1190/geo2023-0224.1

low-frequency ground resistivity survey and confirmed by drilling (Kaminski et al., 2011).

DATA INVERSIONS

Conjugate gradient adaptive unconstrained 1D inversion

A nonlinear least-squares iterative 1D inversion algorithm based on the conjugate gradient method with the adaptive regularization and weighting of the inverted parameters (Zhdanov, 2002) can be used to invert apparent conductivities derived from the natural EM fields variations data. This is most useful for the rapid generation of resistivity depth images. These can be used for preliminary interpretation and to identify "bad points" induced by external noise sources or associated with low-amplitude natural fields at one or more frequencies. The depth images also can be used to select data for further inversions and preliminary estimation of the depth of investigation based on the sensitivity or Jacobian matrix (Christiansen and Auken, 2012). If applicable, the 1D model can be further used for developing a data static correction strategy.

MARE2DEM nonlinear adaptive finite-element inversion

MARE2DEM is a freely available source code based on a goal-oriented adaptive finite-element algorithm that computes highly accurate solutions for 2.5D MT problems (Key, 2016). We have developed tools to generate MobileMT data input files and develop unstructured triangular element grids for all survey lines to use in the MARE2DEM code. This enables the inversion of large amounts of airborne electromagnetic data. The 2021 version of MARE2DEM is capable of handling MobileMT data specifically because it includes the option of a stationary base used as the E-field for all measurement stations along a survey line.

The unstructured finite-element triangular grids (meshes) provide high geometric flexibility during the inversion process. This way of subsurface media discretization is highly efficient in modelling complex and highly variable structures (Key and Weiss, 2006) and relevant to MobileMT total-field data because it is sensitive to geoelectrical boundaries at any orientation.

FIELD EXAMPLES

Almost all field examples presented here are taken from MobileMT surveys conducted as part of exploration programs for various commodities, such as critical minerals. The case study of a known kimberlite pipe in Ontario, however, is based on data acquired during a test survey.

This case study example in which we use the 1D inversion of apparent conductivity data, and all others presented, use MARE2DEM. A uniform half-space was the starting model for all the 1D and 2D inversions of the processed apparent conductivity data.

Lake Timiskaming kimberlite field (north-eastern Ontario, Canada)

The KL-01 kimberlite was discovered, along with other pipes, in the Klock and van Nostrand townships by Contact Diamond Corp. in 2004, using a combination of till sampling and geophysical methods. The Geological Survey of Canada also studied the kimberlite pipe in 2005, using volcanoclastic kimberlite breccia samples from diamond drill core (McClenaghan et al., 2008). The KL-01 kimberlite is covered by 1–4 m of till, as noted by McClenaghan et al. (2008), but according to the core logging from hole KL01-1, the thickness of overburden/boulders is 13.7 m (Sobie, 2004). The bedrock geology in the vicinity of the kimberlite consists of Paleoproterozoic rocks of the Lorrain and Gowganda formation. The kimberlite body (approximately 150 m × 300 m) has an elongated morphology following an azimuth at 325° parallel to the trend of the Kerry Lake fault (McClenaghan et al., 2008).

In 2021, Expert Geophysics Limited flew a test survey over the KL-01 and KL-22 kimberlite pipes with a modified system called MobileMTm that has a GPS antenna and two magnetic sensors on the same housing (bird) that are used for the three inductive receiver coils. The effective areas of the inductive coils and the total weight of the towed system are reduced versus a standard MobileMT. Results of the survey over the KL-22 pipe are presented by Prikhodko et al. (2022). This paper presents the results for KL-01, located 5 km from KL-22. The positions of the historic drillholes are presented over an image of the MobileMT apparent conductivity calculated from the 5381 Hz data (Figure 6). Of the two drillholes, KL01-D4 and KL01-1 intersected hypabyssal kimberlite (containing baked and concentrically zoned limestone xenoliths), and KL01-1 intersected tuffisitic kimberlite breccia with nonmagmatic inter clast matrix below 375 m ASL.

The one-dimensional inversions used the same starting model for each measurement station. All 200 layers had a thickness of 20 m, and the resistivity of all layers was set to the average resistivity for all 16 accepted frequencies (in the range 102–17,099 Hz) along line L4060 (location shown in Figure 6). The estimated logarithmic convergence (e^{ln}), as defined by Zhdanov (2009), is the square of the difference between the natural logarithm of the observed (obs) and predicted (pr) resistivity data. This quantity was generally between 0.0145–0.0178 (Figure 7), considering these fits reasonable for MobileMT data. The data inversion results demonstrate the MobileMT system's capability to detect the kimberlite pipe.

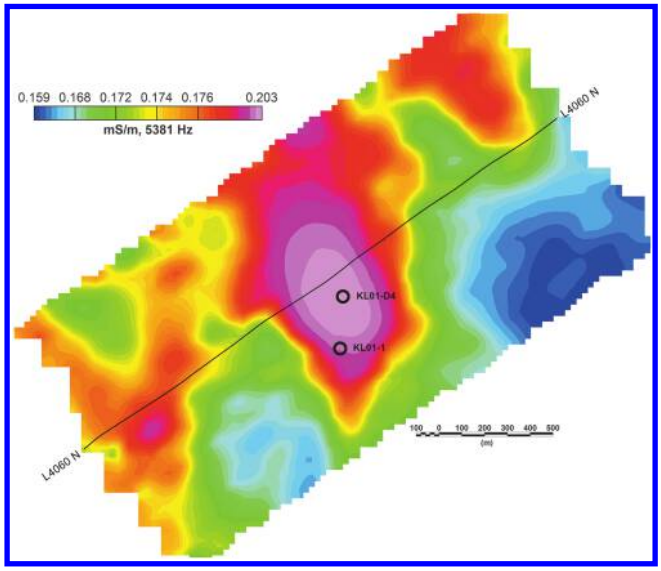

Figure 6. Color grid of the apparent conductivity calculated from 5381 Hz data over the area around the KL-01 kimberlite pipe, with the position of drillholes and the survey line L4060.

Athabasca basin (Canada, mono- and polymetallic unconformity-associated uranium mineralization)

The Athabasca basin contains diverse deposits in terms of their shapes, sizes, and compositions, and has been reviewed by Jefferson et al. (2007). These deposits can range from uranium monometallic veins "ingress style", typically found in the basement, to polymetallic (complex) lenses located just above or straddling the unconformity (U/C) "egress style". The mineralization can contain varying amounts of Ni, Co, As, Pb, and trace amounts of Au, Pt, Cu, REEs, and Fe. The deposits often are associated with the highly conductive graphitic zones below the U/C. Weakly conductive clay alteration features or highly resistive silicification in the overlying sediments can indicate the alteration that accompanies the deposits (Mwenifumbo et al., 2004).

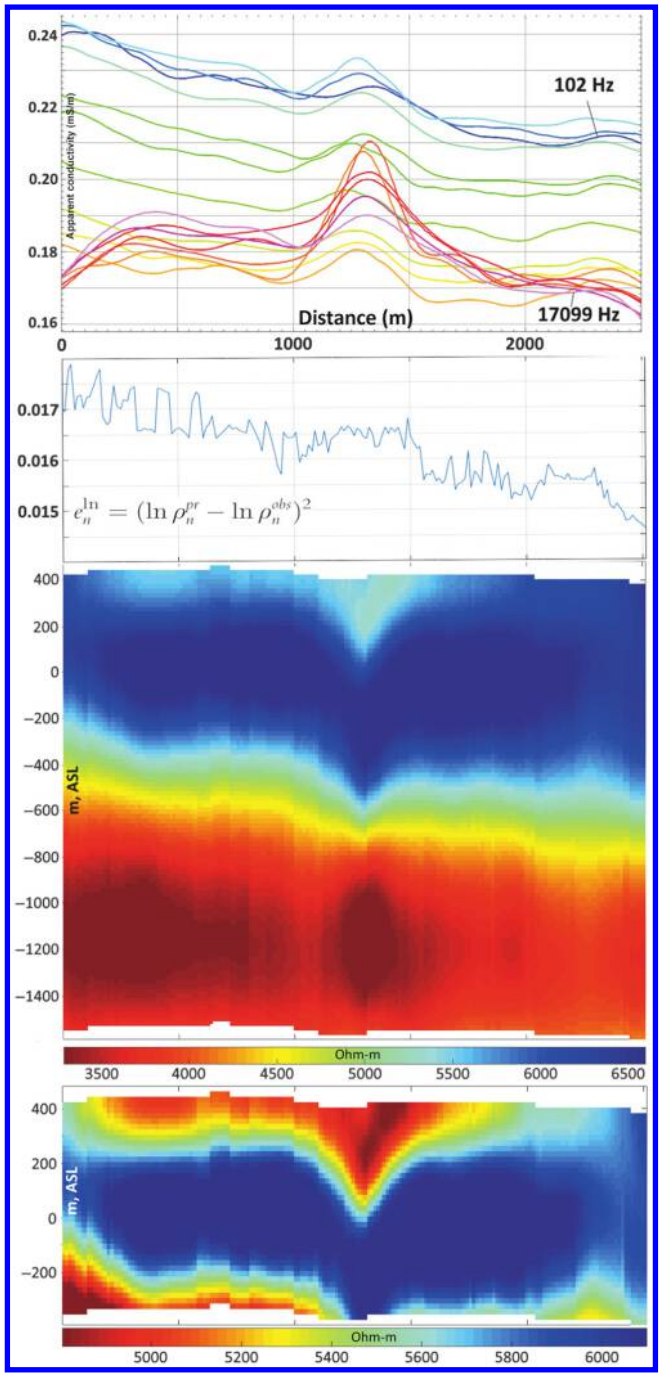

Figure 7. Example of MobileMT data inversion with 1D layered earth model along a survey line L4060 crossing KL-01 kimberlite pipe (Ontario). From top to bottom: MobileMT apparent conductivity data for a set of frequencies from 102 Hz to 17,099 Hz; log convergence profile; inverted resistivity-depth image up to 2 km depth from the surface; inverted resistivity-depth image up to 800 m depth from the surface.

Figure 8 shows, in the top part, the project area (from the Virgin River shear zone) with the vertical derivative of the magnetics and conductive structures (red lines). The map is taken from Baselode Energy Corp. (2020). Also marked on the map is the location of two lines, L3760 and L3840. The bottom part of Figure 8 shows the resistivity section derived from 2D inversions for L3760 and two conductive structures (A1 and A2) marked in the section. The right structure A2 is indicated to outcrop. These structures have been interpreted to be approximately 600 m apart along this line. They were mapped across a strike length of approximately 7 km and are identified as fault zones with depths of up to 1 km. The MobileMT data revealed "bifurcating and subparallel structures that were previously not observed" (Baselode Energy Corp., 2020). Structures such as these were considered prospective for uranium and were "targeting vectors" for an "upcoming drill campaign" (Baselode Energy Corp., 2020). This field example highlights how the MobileMT system can resolve two conductors about 600 m apart, one of which is indicated to outcrop and could extend to approximately 1 km deep. It also illustrates how the data can advance an exploration program.

The case study presented in Figure 9 shows another case from the Athabasca Basin, located between the McArthur River Mine and the Millennium deposits in the southeastern part of the basin. The position of the U/C is confirmed by a drillhole drilled after the airborne EM survey (Figure 9). The MobileMT data enables the identification of surficial moderately conductive quaternary glacial till sediments, highly resistive Paleoproterozoic Athabasca Group sandstones, and conductive Archean to Paleoproterozoic graphitic faults in the basement. The top of the conductive material in the basement provides a reasonable estimate for the U/C depth, as confirmed by drilling shown in Figure 9 (Basin Uranium Corp., 2023).

Kendyktas Ridge (Southern Kazakhstan, epithermal polymetallic deposits)

Copper, copper-gold, and copper-molybdenum deposits in the Kendyktas Ridge (Central Asian Ordovician magmatic arc) in south-central Kazakhstan are commonly associated with stockwork style and veins (Zientek et al., 2014). The region hosts several typical deposits, such as Chatyrkul (544,200t of copper), Jaisan, Ungurli, and Aktasty. Approximately half of the mineralization in the deposits is associated with metasomatically altered granitoids, and half occurs as quartz-chalcopyrite and quartz-calcite-chalcopyrite veins. The known deposits in the region are positioned over subalkaline intrusives of Devonian age (Zhadrinsky intrusive complex), which underly the older late Ordovician granites in the areas of the Ungurli ore field and the Jaisan deposit. The Devonian subalkaline intrusive rocks were defined as highly resistive from the results of historical IP surveys in the region. The

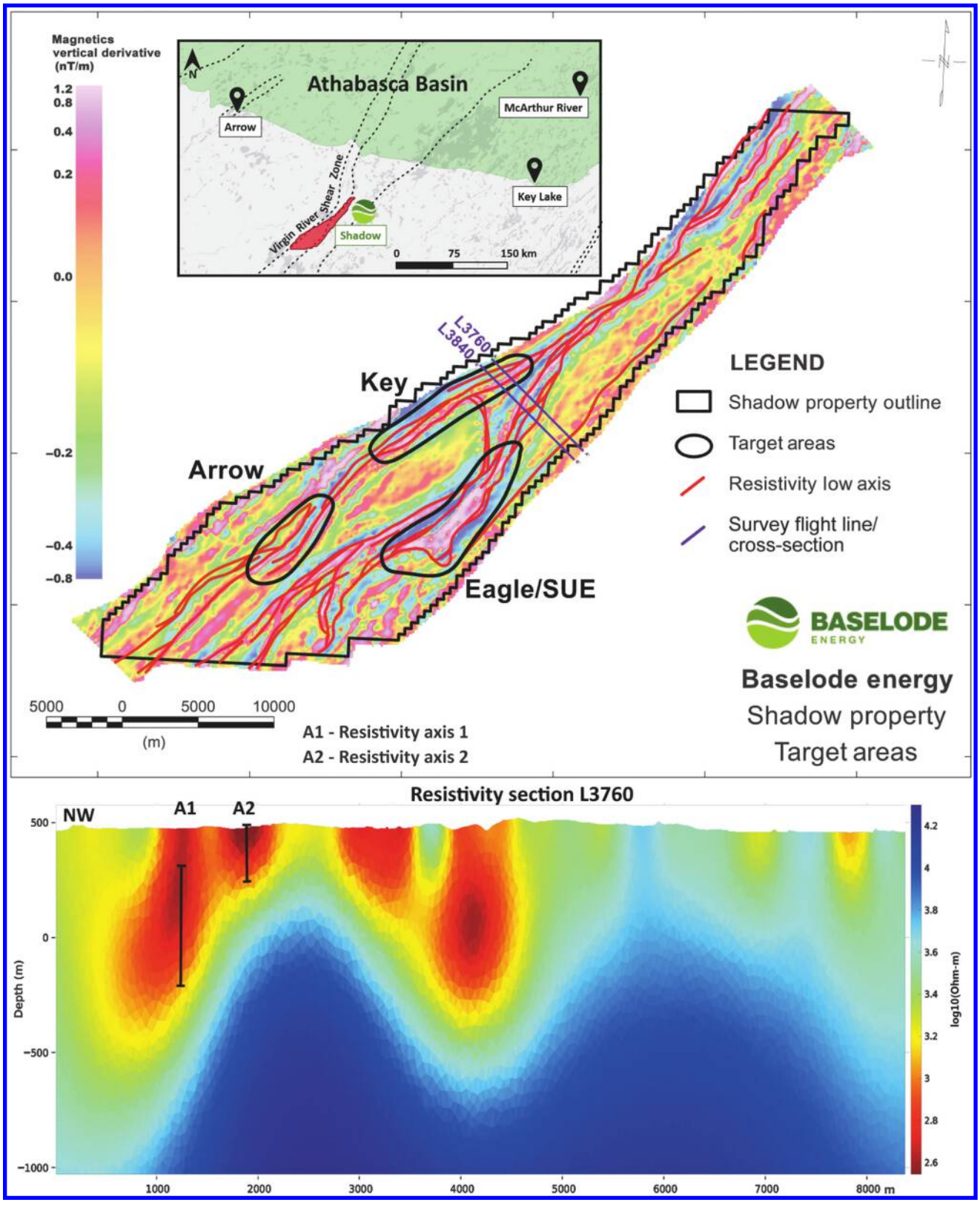

Figure 8. Map of the survey area showing the vertical derivative of the magnetics, conductive axes, and the location of profiles L3760 and L3840 (top). The resistivity section along MobileMT survey line L3760 showing the ability to resolve two separate conductors about 600 m apart (reinverted in 2D and modified from Baselode Energy Corp., 2020).

DOI:10.1190/geo2023-0224.1

DOI:10.1190/geo2023-0224.1

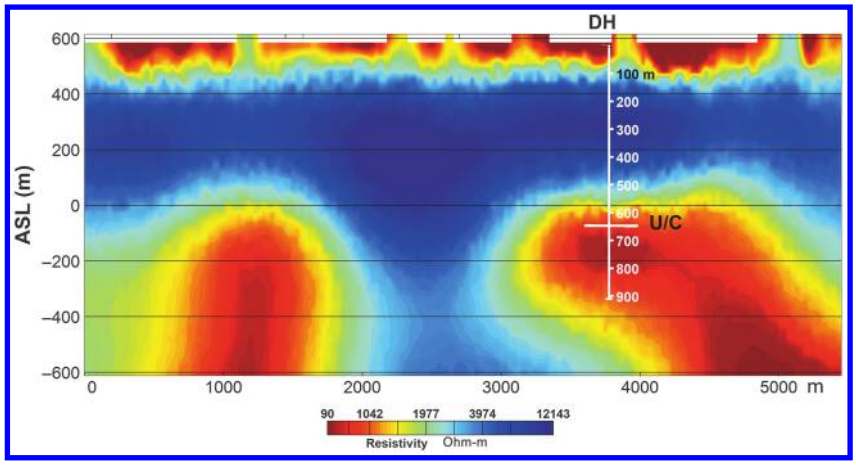

Figure 9. Resistivity-depth section along a survey line in the eastern part of the Athabasca Basin with a drillhole position showing the U/C and conductors clearly mapped below the U/C.

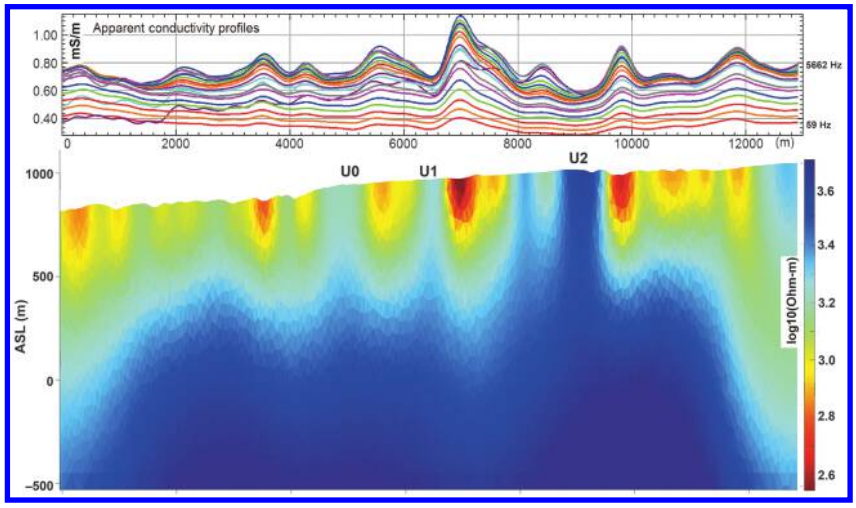

Figure 10. Apparent conductivity profiles and resistivity section along a line crossing known ore zones (U0, U1, and U2) of the epithermal deposit Ungurli in the area of Kondyktas Ridge.

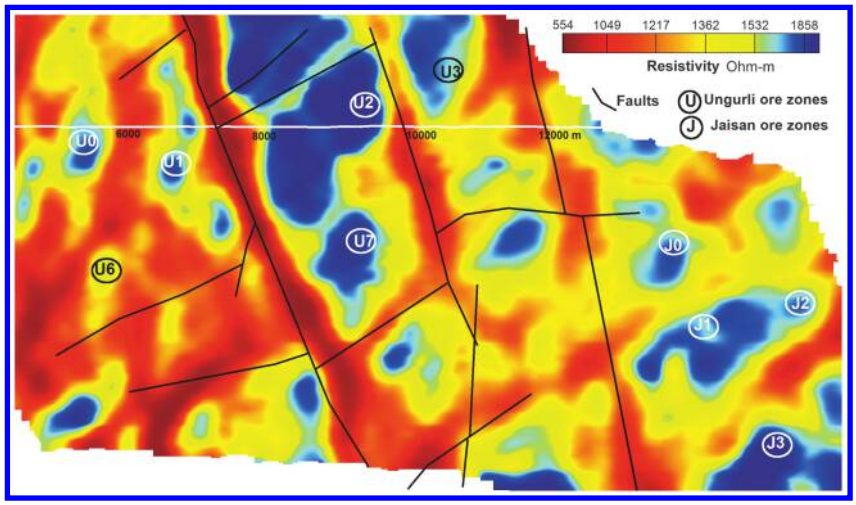

Figure 11. Resistivity-depth slice corresponded to 750 m ASL also showing the position of the survey line from Figure 10, positions of known ore zones from Ungurli and Jaisan deposits, and geologically mapped faults.

results of the MobileMT survey show electrically resistive dome structures at depth, which are interpreted as intrusives of the Zhadrinsky complex and resistive "vents" resembling a vertical pipe that coincides with the position of the known ore zones of the Ungurli Cu-Mo-Au deposit (Figure 10). A plan view of the survey at a depth slice of 750 m ASL (Figure 11) shows resistive features associated with ore zones of the Ungurli and the Jaisan deposits. The resistive features in Figure 10 are similar in form to those on a conceptual geologic model (Figure 12) of magmatic-hydrothermal systems that produce porphyry and related epithermal ore deposits. The model developed by Heinrich (2005) is based on general geologic observations, experimental thermodynamic data, and quantitative fluid inclusion microanalyses of mineral systems worldwide.

This case study exemplifies the ability of natural-field airborne electromagnetic technology to identify deep and near-surface petrophysical patterns associated with structures that control mineralization.

Uspensky rift ore belt (Central Kazakhstan, ferromanganese and polymetallic ores)

The mineralization type in the Uspensky continental rift valley comprises Fe-Mg stratiform lenses, with superimposed polymetallic zinc, lead, barium, copper and associated mercury, cadmium, silver, antimony, thallium, indium occurring at the comparatively near-surface contact between the volcano-sediment layers and the overlying alluvium (Askarova et al., 2021). The permeable late Devonian tuffs, sandstone, conglomerates, and alevrolites (labeled (D_3fm-a and -b in Figure 13) unconformably overly the middle Devonian alevrolites and sandstones (labeled D_2gv-D_3fr). Quaternary sediments in the area are ubiquitous, with a thickness of up to 25 m. According to the formation conditions, they are divided into alluvial, alluvial-proluvial, deluvial-proluvial, and lacustrine. It is important to note that on the surface conductive salt deposits (salt-pans) are predominant in low-lying areas.

The main ore minerals of the stratiform iron-manganese, and polymetallic lead-zinc-barite and copper ores are interbedded within the porous argillite-siliceous-limestone package of rocks and the minerals include hematite, barite, galenite, sphalerite, pyrite, and chalcopyrite. The mineralization is considered multistaged — hydrothermal-sedimentary, hydrothermal-metasomatic, and hydrothermal — vein (Askarova et al., 2021).

DOI:10.1190/geo2023-0224.1

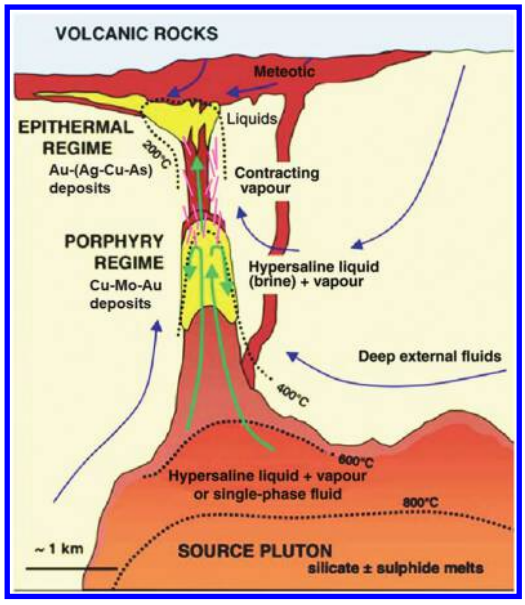

Figure 12. Schematic representation of generalized cross-section model of a magmatic-hydrothermal system (after Heinrich, 2005).

The MobileMT survey, executed in 2022, covered 140 sq. km, including the area of the East Atabay deposit. During the survey, there was a strong signal across the natural electromagnetic spectrum from 22–5662 Hz, and no "dead band" gap near 2000 Hz. Figure 14 shows apparent resistivities, measured (dots) and calculated (lines) corresponding to 20 windows in this frequency range. Each resistivity curve relates to different stations along survey line L1540, which crosses the deposit (Figure 15).

Drilling information has been used to construct a geologic model of the East Atabay deposit. The deposit lies within a Fe-Mg zone stretching from the surface to more than 700 m deep. The copper zone is positioned in the depth range from 300 m to 600 m below the surface (Figure 15). The very near-surface conductors reflect the alluvium sediments and, most likely, a salt-pan on the south end of the line. The other conductive zone below 800 m ASL is in the permeable stratigraphic horizon containing the ore-bearing rocks and is centered on the top of the Cu body identified in the drilling. This case study highlights the ability of the natural field airborne electromagnetic technology to recover complex geologic structures, distinguish between conductors at various depth levels, beginning from the near-surface, and also shows an ability to aid in mineral exploration.

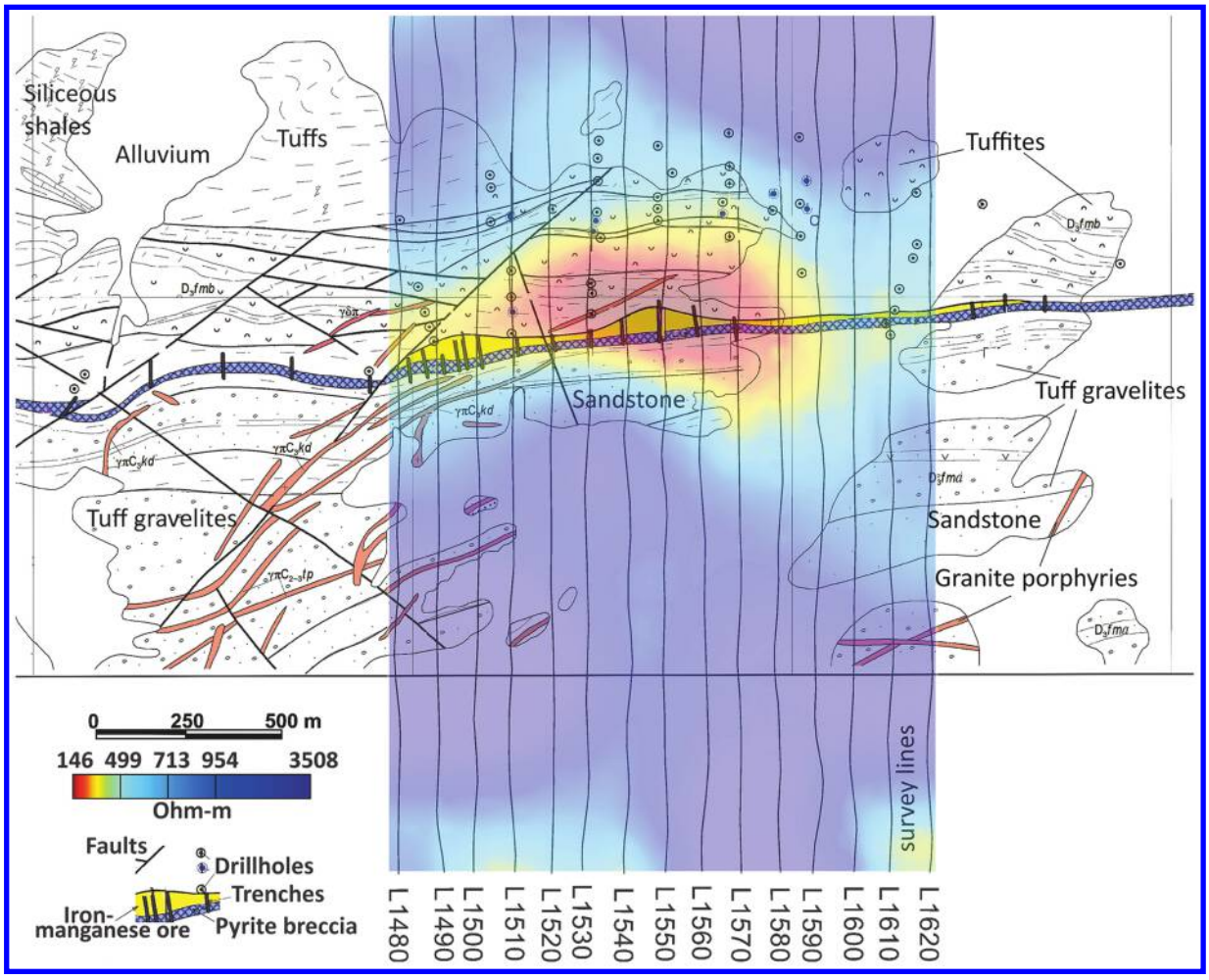

Figure 13. Schematic representation of geologic map and a color map of a resistivity-depth slice at 600 m ASL. The conductive feature in red is ascribed to the East Atabay deposit.

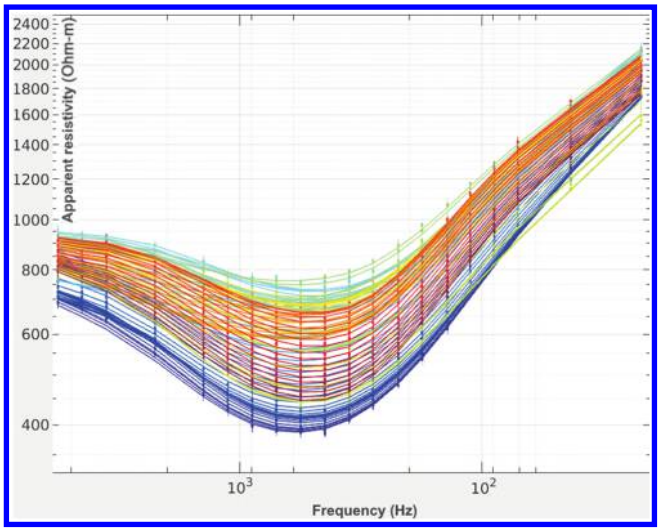

Figure 14. Apparent resistivity curves (dots — observed, lines — modeled) derived from stations along survey line 1540 crossing the East Atabay deposit (Kazakhstan).

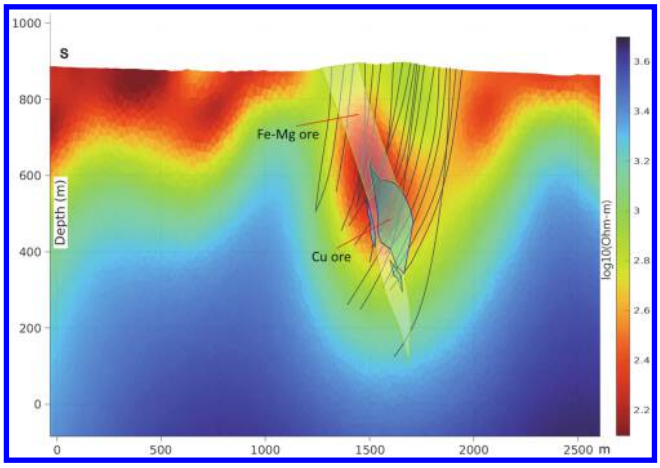

Figure 15. Resistivity-depth section along MobileMT survey line L1540. Also shown are the outlines of the Fe-Mg- and Cu zones as determined from drill information. The drill traces are projected onto the section as shown with the thin curved black lines.

CONCLUSION

Advancements in natural field airborne electromagnetic techniques have resulted in improved exploration abilities. The described "passive" field electromagnetic system measures magnetic and electric field variations in the expanded frequency range that spans three decades of frequency using up to 30 comparatively narrow frequency windows. A mobile receiver measures magnetic-field variations in three orthogonal directions, and a stationary receiver measures electric fields at a base station, including a remote reference set of measurements. The provided case studies illustrate the technology's capacity to investigate depths from near-surface up to more than 1 km. They also demonstrate its capability to identify geoelectrical boundaries of different geometries and detect resistivity differentiations across a wide range of resistivities. In the examples we have presented, the resistivities are as low as 45 Ωm (Figure 4) and as high as 20,000 Ωm (Figure 8). The system has successfully detected known reserves or prospects at the East Atabay, and Ungurli, and a kimberlite pipe. The Atabay deposit, KL-01 pipe and the depth to the top of the conductor below the U/C in the eastern Athabasca have all been drill tested. The high spatial resolution of the passive field system was demonstrated by a survey over comparatively thin subvertical conductors with a recovered thickness of 200 m in the Virgin River shear zone and over 150–200 m width of the kimberlite pipe. Although the electrical resistivity of rocks and minerals can exhibit wide variation, the broadband airborne electromagnetic technology can be useful provided that the petrophysical differences occur within the range covered by the depth of investigation and measured frequency range.

ACKNOWLEDGMENTS

We thank Baselode Energy Corp., Promiseland Exploration, and other companies for giving permission to use their data and providing additional related information. We acknowledge Expert Geophysics Limited technical staff, field crews, data processors, M. Kuzmin, and A. Sirohey personally for their contributions to developments and surveys support. The technique and instrumentation described in the paper were developed with the invaluable methodological guidance and support of P. Kuzmin. N. Golubev developed the 1D data inversion software and adopted the 2D inversion code. We are grateful to A. Carpenter, editors and all anonymous reviewers for reading the manuscript and for their constructive and valuable reviews and suggestions.

DATA AND MATERIALS AVAILABILITY

No data have been required for this paper.

REFERENCES

Allard, M., 2007, On the origin of the HTEM species, *in* B. Milkereit, ed., Proceedings of Exploration 07: Fifth Decennial International Conference on Mineral Exploration, 355–374.

Anav, A., S. Cantarano, P. Cerruli-Irelli, and G. V. Pallotino, 1976, A correlation method for measurement of variable magnetic fields: IEEE Transactions on Geoscience Electronics, **14**, 106–114, doi: 10.1109/TGE.1976.294418.

Annan, P., R. Smith, J. Lemieux, M. O'Connell, and R. Pedersen, 1996, Resistive-limit, time-domain AEM apparent conductivity: Geophysics, **61**, 93–99, doi: 10.1190/1.1443960.

Askarova, N. S., A. T. Roman, V. S. Portnov, and A. N. Kopobayeva, 2021, Feature space of the Atasu type deposits (Central Kazakhstan): Naukovyi Visnyk Natsionalnoho Hirnychoho Universytetu, **5**, 5–10.

Baselode Energy Corp., 2020, News release: Baselode announces results of Mobile MT surveys on the shadow uranium project, November 2, 2020, https://baselode.com/news/baselode-announces-results-of-mobile-mt-survey-on-the-shadowuranium-project/, accessed 26 July 2023.

Basin Uranium Corp., 2023, News release: Basin Uranium continues to intersect anomalous uranium mineralization at Mann Lake, March 7, 2023, https://basinuranium.ca/basin-uranium-continues-to-intersect-anomalous-uranium-mineralization-at-mann-lake/, accessed 6 September 2023.

Cantwell, T., 1960, Detection and analysis of low frequency magnetotelluric signals: Ph.D. thesis, Massachusetts Institute of Technology.

Christiansen, A. V., and E. Auken, 2012, A global measure for depth of investigation: Geophysics, **77**, no. 4, WB171–WB177, doi: 10.1190/geo2011-0393.1.

Heinrich, C. A., 2005, The physical and chemical evolution of low-salinity magmatic fluids at the porphyry to epithermal transition: a thermodynamic study: Mineralium Deposita, **39**, 864–889, doi: 10.1007/s00126-004-0461-9.

Jansen, J. C., and J. A. Cristall, 2017, Mineral exploration using natural EM fields, *in* V. Tschirhart and M. D. Thomas, eds., Targeting 2: Mine to Camp Scale, 349–377.

Jefferson, C. W., D. J. Thomas, S. S. Gandhi, P. Ramaekers, G. Delaney, D. Brisbin, C. Cutts, D. Quirt, P. Portella, and R. A. Olson, 2007, Unconformity associated uranium deposits of the Athabasca Basin, Saskatch-

ewan and Alberta, *in* W. D. Goodfellow, ed., Mineral deposits of Canada: A synthesis of major deposit-types, district metallogeny, the evolution of geological provinces, and exploration methods: Geological association of Canada, Mineral Deposits Division, special publication No. 5, 273–305.
Jones, A. G., 2017, Magnetotellurics: Status Quo and Quo Vadimus: Proceedings of Exploration 17: Sixth Decennial International Conference on Mineral Exploration, 139–158.
Kaminski, V., A. Prikhodko, and D. W. Oldenburg, 2011, Using ERA low frequency E-field profiling and UBC 3D frequency-domain inversion to delineate and discover a mineralized zone in Porcupine district: 81st Annual International Meeting, SEG, Expanded Abstracts, 1262–1266, doi: 10.1190/1.3627433.
Key, K., 2016, MARE2DEM: A 2-D inversion code for controlled-source electromagnetic and magnetotelluric data: Geophysical Journal International, **207**, 571–588, doi: 10.1093/gji/ggw290.
Key, K., and C. Weiss, 2006, Adaptive finite-element modeling using unstructured grids: The 2D magnetotelluric example: Geophysics, **71**, no. 6, G291–G299, doi: 10.1190/1.2348091.
Kuzmin, P. V., G. Borel, E. B. Morrison, and J. Dodds, 2010, Geophysical prospecting using rotationally invariant parameters of natural electromagnetic fields: U. S. Patent 8,289,023.
Labson, V. F., A. Becker, H. F. Morrison, and U. Conti, 1985, Geophysical exploration with audiofrequency natural magnetic fields: Geophysics, **50**, 656–664, doi: 10.1190/1.1441940.
Legault, J., and K. Fisk, 2012, Statement of capability — Geotech Airborne Ltd, *in* R. J. Lane, ed., Abstracts from the ASEG Natural fields EM forum: Geoscience Australia Record 2012/04, 10–21.
Legault, J. M., H. Kumar, B. Milicevic, and L. Hulbert, 2009, ZTEM airborne tipper AFMAG test survey over a magmatic copper-nickel target at Axis Lake in Northern Saskatchewan: 79th Annual International Meeting, SEG, Expanded Abstracts, 1272–1276, doi: 10.1190/1.3255083.
Lo, B., J. Legault, P. Kuzmin, and M. Combrinck, 2009, Z-TEM (airborne AFMAG) tests over unconformity uranium deposits: 20th International Geophysical Conference and Exhibition, ASEG, Extended Abstracts, doi: 10.1071/ASEG2009ab054.
McClenaghan, M. B., I. M. Kjarsgaard, and B. A. Kjarsgaard, 2008, Indicator mineralogy of the KL-01 and KL-22 kimberlites, Lake Timiskaming kimberlite field, Ontario: Open File 5800, Geological Survey of Canada.
Moul, F., and K. Witherly, 2020, A comparison of MobileMT with ZTEM and HeliTEM over isolated conductors in the Athabasca Basin, Saskatchewan, Canada: 90th Annual International Meeting, SEG, Expanded Abstracts, 1389–1393, doi: 10.1190/segam2020-3428466.1.
Mwenifumbo, C. J., B. E. Elliott, C. W. Jefferson, G. R. Bernius, and K. A. Pflug, 2004, Physical rock properties from the Athabasca Group: designing geophysical exploration models for unconformity uranium deposits: Journal of Applied Geophysics, **55**, 117–135, doi: 10.1016/j.jappgeo.2003.06.008.
Prikhodko, A., A. Bagrianski, P. Kuzmin, and A. Sirohey, 2022, Natural field airborne electromagnetics — History of development and current exploration capabilities: Minerals, **12**, 583, doi: 10.3390/min12050583.
Sattel, D., K. Witherly, and V. Kaminski, 2019, A brief analysis of MobileMT data: 89th Annual International Meeting, SEG, Expanded Abstracts, 2138–2142, doi: 10.1190/segam2019-3215437.1.
Smith, R., 2001, On removing the primary field from fixed-wing time-domain airborne electromagnetic data: Some consequences for quantitative modelling, estimating bird position and detecting perfect conductors: Geophysical Prospecting, **49**, 405–416, doi: 10.1046/j.1365-2478.2001.00266.x.
Smith, R., and P. Annan, 1998, The use of B-field measurements in an airborne time-domain system: Part I. Benefits of B-field versus dB/dt data: Exploration Geophysics, **29**, 24–29, doi: 10.1071/EG998024.
Sobie, P., 2004, Report on 2003-2004 exploration on the Klock property Larder Lake mining division, Northeastern Ontario of Sudbury contact mines limited: MPH Consulting Limited.
Vozoff, K., 1972, The magnetotelluric method in the exploration of sedimentary basins: Geophysics, **37**, 98–141, doi: 10.1190/1.1440255.
Zhdanov, M. S., 2002, Geophysical inverse theory and regularization problems: Elsevier, 36.
Zhdanov, M. S., 2009, Geophysical electromagnetic theory and methods: Elsevier, 43.
Zientek, M., J. Hammarstrom, and K. Johnson, 2014, Porphyry copper assessment of Western Central Asia: USGS scientific investigations report 2010-5090-N.

Biographies and photographs of the authors are not available.